Thermodynamic Analysis of Conserved Loop−Stem Interactions in P1−P2 Frameshifting RNA Pseudoknots from Plant *Luteoviridae*†

Paul L. Nixon,‡ Peter V. Cornish, Saritha V. Suram, and David P. Giedroc*

Department of Biochemistry and Biophysics, Center for Advanced Biomolecular Research, Texas A&M University, College Station, Texas 77843-2128

Received March 20, 2002; Revised Manuscript Received June 19, 2002

ABSTRACT: The RNA genomes of plant luteovirids beet western yellows virus (BWYV), potato leaf roll virus (PLRV), and pea enation mosaic virus (PEMV RNA1; PEMV-1) contain a short mRNA pseudoknotted motif overlapping the P1 and P2 open reading frames required for programmed −1 mRNA ribosomal frameshifting. The relationship between structure, stability, and function is poorly understood in these RNA systems. A m^5-C_8-substituted BWYV RNA is employed to establish that the BWYV P1−P2 pseudoknot is protonated at cytidine 8 in loop L1 ($\delta_{N_3H^+}$ = 12.98 ppm), which stabilizes a C^+·(G−C) major groove base triple by $\Delta(\Delta G_{37})_{protonation}$ = 3.1 (±0.4) kcal mol^{-1}. The stabilities of both the PLRV and PEMV-1 P1−P2 pseudoknots are also strongly pH-dependent, with $\Delta(\Delta G_{37})_{protonation}$ = 2.1 (±0.2) kcal mol^{-1} for the PEMV-1 pseudoknot despite a distinct structural context. As previously found for the BWYV pseudoknot [Nixon and Giedroc (2000) *J. Mol. Biol. 296*, 659], both the PLRV and PEMV-1 RNAs are stabilized by $\Delta H \geq 30$ kcal mol^{-1} in excess of secondary structure predictions, attributed to loop L2−stem S1 minor groove triplex interactions. BWYV RNAs containing single 2′-deoxy or A → G substitutions that disrupt L2−S1 hydrogen bonding are strongly destabilized with $\Delta(\Delta G_{37})_{folding}$ (pH = 7.0) ranging from ≈1.8 (±0.3) to ≥4.0 kcal mol^{-1}, relative to the wild-type BWYV RNA. These findings suggest that each member of this family of pseudoknots adopts a tightly folded structure that maximizes the cooperativity and complementarity of L1−S2 and L2−S1 loop−stem interactions required in part to offset the low intrinsic stability of the short three base pair pseudoknot stem S2.

Programmed −1 ribosomal mRNA frameshifting is employed by RNA viruses and retrotransposable elements to synthesize structural proteins relative to replicative enzymes encoded in overlapping open reading frames by way of a single translation initiation event (for reviews, see refs *1*−*4*). Specific sequence and structural requirements are known to be required to stimulate high levels of translational reprogramming via −1 frameshifting of the elongating ribosome. Originally proposed in the simultaneous slippage model (*5*), the ribosome must encounter a "slippery site" of the general sequence X XXY YYZ which stimulates both ribosomal pausing and slippage (*6*, *7*). While the presence of a slip site in an mRNA imparts a low level of background −1 ribosomal frameshifting, high levels of recoding require the presence of an RNA secondary structure, typically a hairpin-type RNA pseudoknot, optimally positioned six to eight nucleotides downstream of the slip site (*4*).

Although the mechanism by which pseudoknots stimulate −1 ribosomal frameshifting remains elusive, a range of pseudoknot topologies appear capable of stimulating recoding. These pseudoknots can be grouped into four basic classes, each characterized by distinct structural and sequence requirements for mRNA frameshifting (*4*). The P1−P2 frameshifting pseudoknot from the plant luteovirus beet western yellows virus (BWYV)[1] is representative of one such class (Figure 1). From polymer prediction theories (*8*), the BWYV pseudoknot is predicted to be weakly folded in the absence of additional stabilizing loop−stem interactions beyond that established by Watson−Crick base stacking, base pairing, and potential stacking of pseudoknot helical stems, due principally to a short helical stem S2 (Figure 1). Consistent with this prediction, the crystallographic structure of the BWYV pseudoknot reveals significant loop−stem interactions previously not observed in simple H-type pseudoknots (*9*). Three stacked adenosines found at the 3′ end of loop L2 form a number of hydrogen-bonding interactions to 2′-OH groups and the minor groove faces of a pair of conserved G-C base pairs derived from stem S1, which are expected to be strongly stabilizing (*10*). A cytidine from loop L1 (C_8) was also found to make hydrogen-bonding interactions with the major groove face of a G-C base pair in stem S2 (G_{12}-C_{26}) to form a protonated C^+·(G-C) Hoogsteen-type base triple. The structure of this triple is analogous to that found in the HDV ribozyme (*11*, *12*), and protonation contributes ≈3.5 kcal mol^{-1} to the stability of

† This work was supported by grants from the NIH (AI40187) and the Texas Higher Education Coordinating Board Advanced Research Program (010361-0278-1999). P.V.C. was supported in part by an NIH Chemistry−Biology Interface Training Grant (T32 GM08523).

* Corresponding author. E-mail: giedroc@tamu.edu. Telephone: 979-845-4231. Fax: 979-845-4946.

‡ Current address: Department of Biochemistry, University of Texas Southwestern Medical Center at Dallas, 5323 Harry Hines Blvd., Dallas, TX 75390-9038.

[1] Abbreviations: BWYV, beet western yellows virus; DSC, differential scanning calorimetry; PEMV, pea enation mosaic virus; PEMV-1, genomic RNA1 of PEMV; PLRV, potato leaf roll virus.

10.1021/bi025843c CCC: $22.00
Published on Web 08/02/2002

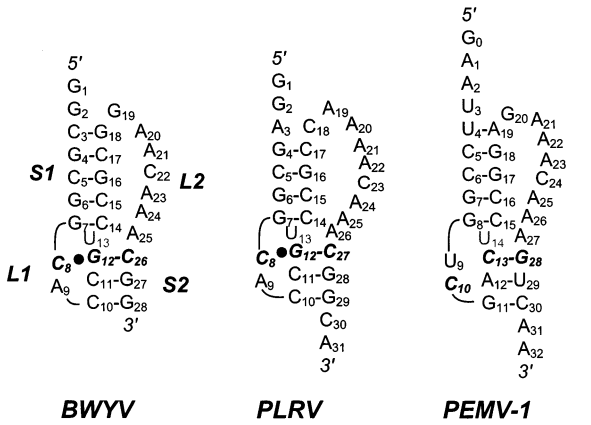

FIGURE 1: Secondary structural schematic representations of the plant luteoviral family of P1−P2 frameshifting pseudoknots from beet western yellows virus (BWYV), potato leaf roll virus (PLRV), and pea enation mosaic virus 1 (PEMV-1). Nucleotides involved in formation of the C^+•(G-C) base triple in the BWYV and PLRV pseudoknots are shown in bold italics; note that the nucleotide sequences of loop L1 and stem S2 are different in PEMV-1 (see text for details). The uridine at the helical junction (shaded) is unpaired and extruded from the helix in the BWYV (*9*) and PEMV-1[2] pseudoknots.

the folded RNA (*13*). The C^+•(G-C) base triple as well as the minor groove adenosine triplex motif has been shown to be absolutely required to stimulate −1 frameshifting (*9*).

BWYV is a member of plant *Luteoviridae*, a large group of aphid-transmissible RNA viruses (for a review, see ref *14*). The genomes of the polerovirus potato leaf roll virus (PLRV) and the luteovirus barley yellow dwarf virus (BYDV) (*22*), as well as RNA1 of pea enation mosaic virus (PEMV-1), all encode P1−P2 pseudoknots expected to be similar to that of BWYV (cf. Figure 1); all have been shown to stimulate modest levels of −1 ribosomal mRNA frameshifting in vitro and in vivo (*15*−*19*).[2] Of particular interest here is the PEMV-1 RNA, which incorporates base substitutions that would be predicted to impair formation of a BWYV-like Hoogsteen C^+•(G-C) base triple (Figure 1).

As first pointed out by Puglisi et al. (*20*), the pseudoknotted conformation is in equilibrium with the partially folded stem S1 and stem S2 stem−loop structures in a manner governed by the relative free energies of the different states (for a review, see ref *4*). Plant *Luteoviridae* pseudoknots are universally characterized by pseudoknot S2 stems that lack sufficient length (three base pairs) to easily overcome the entropic barrier to closing two pseudoknot loops (*8*). In this paper, we present NMR and thermodynamic evidence supporting the proposal that all luteovirid P1−P2 pseudoknots adopt folded structures that maximize cooperativity and complementarity of pseudoknot loop−stem interactions that are required to stabilize the pseudoknotted conformation relative to partially folded and functionally inactive stem−loop structures.

MATERIALS AND METHODS

RNA Synthesis and Purification. RNA transcripts corresponding to the minimal sequences of the PLRV and PEMV-1 P1−P2 frameshifting RNA pseudoknots and pseudoknot mutants (cf. Figure 1) were synthesized using in vitro transcription under control of the SP6 promoter from fully double-stranded oligonucleotide templates essentially as described previously (*21*). SP6 RNAP was purified from *Escherichia coli* BL21(DE3) transformed with pSR3 using the method described by Jorgensen et al. (*22*) but with the final gel filtration column omitted. Wild-type, A23G, A24G, and A25G BWYV RNAs were obtained by in vitro transcription of partially double-stranded templates by T7 RNAP or fully double-stranded templates with SP6 RNAP as previously described (*13*, *23*). The m^5-C_8, deoxy-2′-C_{14}, and deoxy-2′-C_{15} BWYV RNAs were obtained as 28-mers (Figure 1) from Dharmacon, deprotected as described by the manufacturer, and purified using denaturing PAGE, electroelution, and C18 chromatography (*13*, *23*).

Sample Preparation. RNAs for optical denaturation studies were resuspended and dialyzed for ≈9 h against three changes of the appropriate buffer. The first buffer change contained 1 mM EDTA to remove divalent ions weakly bound to the RNAs. Samples for analysis by differential scanning calorimetry (DSC) were further dialyzed for more than 16 h against the final change of dialysis buffer. Buffers used for the calorimetry and optical denaturation studies were made 0.5 M KCl and 10 mM in buffer component as follows: acetate, pH 4.5 and 5.0; Mes, pH 5.5 and 6.0; Mops, pH 6.5 and 7.0; Hepes, pH 7.5 and 8.0; Epps, pH 8.5; and Ches, pH 9.0 (*13*, *24*). NMR samples were prepared by repeated ethanol precipitation in the appropriate buffer to remove residual acrylamide prior to resuspension in a final volume of 300 μL of 100 mM KCl and 10 mM potassium phosphate, pH 6.0, lyophilized overnight, and loaded into Shigemi tubes for NMR analysis.

Optical and Calorimetric Data Collection and Analysis. Optical denaturation profiles were collected on a Cary 1 spectrophotometer equipped with a temperature controller (1−3 μM RNA), and the resulting melting profiles ($\partial A/\partial T$ vs T) acquired at 260 and 280 nm were simultaneously fit to a multiple sequential interacting transition unfolding model using t-melt as described previously (*13*, *25*). Only up-melts were performed, and the temperature ramp rate was 0.3 °C/min from 5 to 95 °C. Reproducibility of melting profiles was assessed from replicate melts. Calorimetrically monitored unfolding profiles were collected on a MicroCal VP DSC from 5 to 120 °C at a ramp rate of 1 °C/min as described previously (*13*, *25*) and analyzed using Origin to a model corresponding to two or three sequential interacting two-state unfolding transitions assuming $\Delta C_p^\circ = 0$. In these fits, the sum of the van't Hoff unfolding enthalpies (ΔH_{vH}) for each transition was constrained to equal ΔH_{cal}, with $\sum \Delta H_{vH} = \sum \Delta H_{cal}$. Total ΔH_{cal} was defined by the integrated area under the reference-subtracted melting curve, with the baseline interpolated using a linear baseline approximation method conservatively estimated from the pre- and post-transition regions, using the optical melting profiles as a guide (*13*).

NMR Data Collection and Analysis. NMR data on the PEMV-1 and BWYV RNA samples were acquired on either a Varian Inova 500 or Varian Inova 600 MHz spectrometer (Biomolecular NMR Laboratory, Texas A&M University) using WATERGATE water suppression. 1D spectra were collected as 256 transients of 2560 complex points over a

[2] The solution structure of the PEMV-1 pseudoknot will be reported in a separate communication [P. L. Nixon, A. Rangan, Y-. G. Kim, A. Rich, D. W. Hoffman, M. Hennig, and D. P. Giedroc (2002) *J. Mol. Biol.* (in press)].

sweep width of 12.5−15 kHz. The 2D spectra of the m^5-C8-BWYV RNA were collected using 64 transients containing 2560 complex points in the directly detected dimension over a 15 kHz sweep width with 340 complex points in the indirectly detected dimension. Data were processed using NMRPipe and visualized using NMRDraw (*26*) or with Sparky, version 3 (SPARKY 3, University of California, San Francisco). All NMR spectra were referenced to DSS.

Analysis of the pH Dependence of Unfolding. $t_{m,i}$ and $\Delta H_{vH,i}$ resolved for the first and second unfolding transitions from optical and calorimetric melting profiles collected as a function of pH were used to calculate ΔS_i from $\Delta S_i = \Delta H_{vH,i}/t_{m,i}$ and $\Delta G_{37,i} = \Delta H_{vH,i} - T\Delta S_i$, where $T = 310$ K. For a simple RNA motif like a pseudoknot, unfolding along the equilibrium coordinate is often well-ordered, with tertiary structure unfolding prior to the unfolding of the helical stems, which unfold in an order governed by their relative secondary structural stabilities (*27*). Thus, tertiary structure can potentially stabilize secondary structure unfolding (*28*), which can effectively increase the cooperativity of unfolding (cf. Results). Since the thermodynamic parameters for the unfolding of stem S1 were found to be independent of pH, the sum of $\Delta G_{37,i}$ for the first and second unfolding transitions ($\Delta G_{37,obs} = \Delta G_1 + \Delta G_2$) fully takes this obligatory coupling into account. The pH dependence of $\Delta G_{37,obs}$ was analyzed using a model in which the entire change in $\Delta G_{37,obs}$ as a function of pH is attributed to protonation of a single ionizable group on the RNA characterized by unique pK_a according to

$$\Delta G_{37,obs} = \Delta G_{37}^{\text{unprotonated}} + (\Delta G_{37}^{\text{protonated}} - \Delta G_{37}^{\text{unprotonated}})[10^{pK_a - pH}/(1 + 10^{pK_a - pH})]$$

where $\Delta G_{37}^{\text{protonated}}$ is the $\Delta G_1 + \Delta G_2$ for the protonated RNA and $\Delta G_{37}^{\text{unprotonated}}$ is the $\Delta G_1 + \Delta G_2$ for the unprotonated RNA. This analysis is analogous to that performed previously ($t_{m,1}^{-1}$ vs $[H^+]$) (*13*), except that it more fully accounts for the degree to which protonation stabilizes the RNA.

RESULTS

NMR Structural and Thermodynamic Analysis of the m^5-C_8-BWYV Pseudoknot. Previously, evidence in support of the protonation of N3 of C_8 in solution to form a C_8^+•(G_{12}-C_{26}) base triple in the BWYV pseudoknot was provided by a thermodynamic analysis of the unfolding of U_8 and A_{12}-U_{26} substitution mutant BWYV pseudoknots (*13*). Direct verification of the protonation state of C_8 at pH 6.0 was obtained with a synthetic RNA containing 5-methylcytidine in place of C_8. As described in Figure 2A, analysis of a region of the short mixing time H_2O NOESY spectrum of the m^5-C_8-BWYV RNA (Figure 2A) is fully compatible with the proposed C_8^+•(G_{12}-C_{26}) base triple shown in Figure 2B.

Analysis of the thermodynamics of unfolding of the m^5-C_8-BWYV pseudoknot using optical spectroscopy reveals melting profiles essentially identical to those observed previously (*13*) for the unmodified BWYV pseudoknot (Figure 3). The unfolding of the m^5-C_8-BWYV pseudoknot is modeled well by three sequential two-state unfolding transitions where transition 1 is assigned to the unfolding of the loop−stem interactions (F → PK), transition 2 to the unfolding of the less stable stem S2 (PK → S1), with

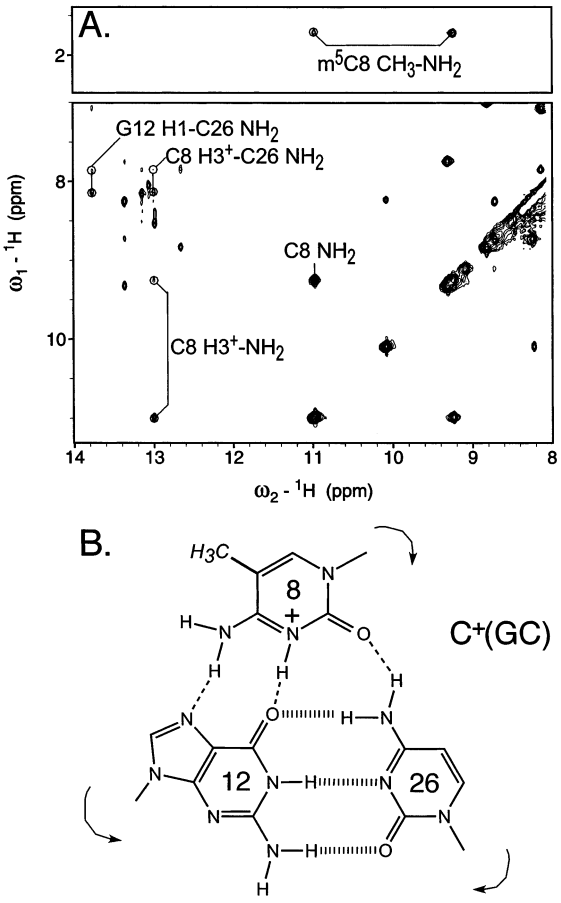

FIGURE 2: (A) 60 ms WATERGATE NOESY spectrum of the m^5-C_8-BWYV pseudoknot (0.8 mM) acquired on a Varian Inova 600 spectrometer at 10 °C, pH 6.0. The methyl protons of m^5-C_8 resonate at 1.73 ppm and exhibit strong cross-peaks to a pair of downfield-shifted amino protons (9.25 and 11.02 ppm) as expected for a cytidine protonated at N3. These m^5-C_8 amino protons have strong cross-peaks to an imino proton at 12.98 ppm, assigned to m^5-C_8^+ H3. Also highlighted are a pair of hydrogen-bonded amino protons (7.85 and 8.15 ppm) which give strong cross-peaks to two imino protons, m^5-C_8^+ H3 (12.98) and another assigned to G_{12} H1 (13.77 ppm) of the accepting C_{12}-G_{26} base pair. (B) Schematic representation of the m^5-C_8^+•(G_{12}-C_{26}) Hoogsteen base triple from the BWYV pseudoknot.

transition 3 corresponding to the unfolding of the more stable stem S1 (S1 → U) (Figure 3). Fitting of the optically monitored denaturation profiles using a sequential interacting three-transition unfolding model suggests little enthalpic destabilization of the loop−stem tertiary structure interactions results upon m^5-C_8 substitution [$\Delta H_{F\rightarrow PK} = 33$ (±5) vs 32 (±7) kcal mol^{-1} for BWYV] (Figure 3, legend) (*13*).

The total change of ΔG_{37} as a function of pH for unfolding of the pseudoknot including the loop−stem interactions (F → PK) and stem S2 (PK → S1) can be used to determine the macroscopic pK_a for those functional group(s) which contribute to the stability of the m^5-C_8-BWYV pseudoknot (*13*, *24*). Note that this pK_a does not necessarily correspond to the microscopic pK_a for N3 of m^5-C_8 under these solution conditions. The pK_a of N3 for free 5-methylcytidine is 0.1−0.2 unit higher than free cytidine (*29*, *30*). Fitting the change of $\Delta G_{37(F\rightarrow S1)}$ as a function of pH for this RNA to a model in which the entire change in ΔG_{37} is attributed to a single protonatable group resolves an apparent p$K_a = 6.7$ (±0.4) for the N3 of 5-methylcytidine in the context of the BWYV

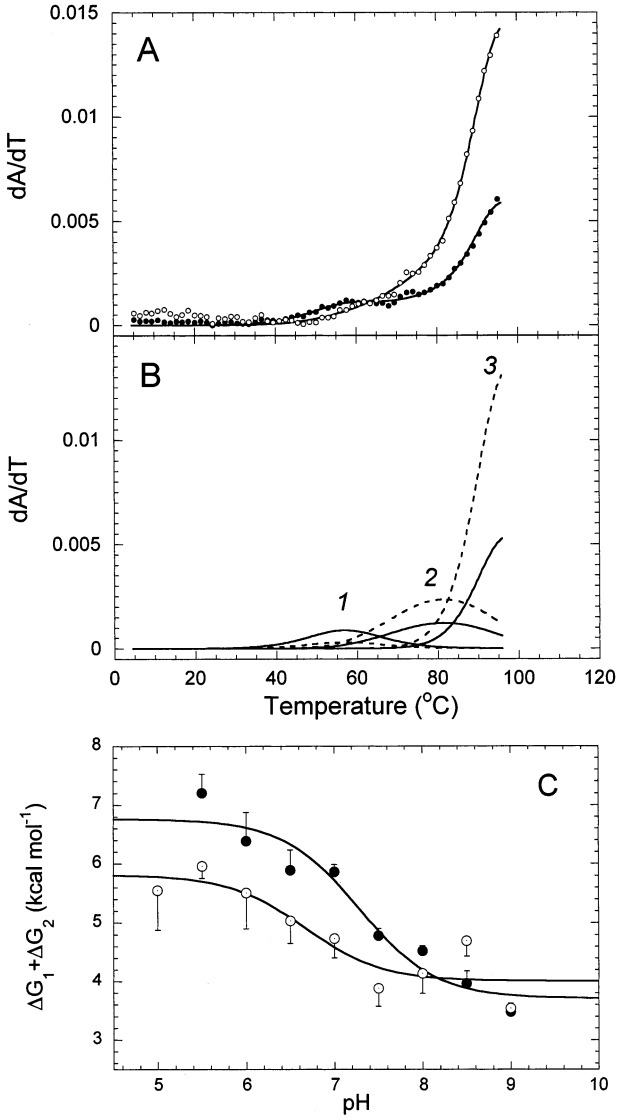

FIGURE 3: (A) Optically monitored unfolding of the m^5-C_8-BWYV pseudoknot at 260 nm (●) and 280 nm (○). The solid lines superimposed on 20% of the experimental data represent a simultaneous fit of the data to a model of three sequential, interacting unfolding transitions. The three unfolding transitions (1, 2, and 3) are attributed to the unfolding of the pseudoknot tertiary structure, stem S2, and stem S1, respectively (*13*). (B) Individual transitions which comprise the composite fit to the data shown in panel A dA_{260}/dT (—), dA_{280}/dT (---). This melting profile is qualitatively similar to the unmodified BWYV pseudoknot (*13*). Calculated values for the fit are as follows: $t_{m1} = 57.3$ °C, $\Delta H_1 = 33.6$ kcal mol^{-1} ($\Delta H_{BWYV} = 32 \pm 7$ kcal mol^{-1}); $t_{m2} = 81.1$ °C, $\Delta H_2 = 29$ kcal mol^{-1} ($\Delta H_{INN-HB} = 26$ kcal mol^{-1}); $t_{m3} = 97.3$ °C, $\Delta H_3 = 47$ kcal mol^{-1} ($\Delta H_{INN-HB} = 50$ kcal mol^{-1}). (C) Analysis of the dependence on solution pH of unfolding of the m^5-C_8-BWYV pseudoknot (○) versus the unmodified BWYV pseudoknot (●). Data shown are the average (±SD) $\Delta G_{37,obs}$ ($\Delta G_1 + \Delta G_2$) from four independent experiments for the first two unfolding transitions (F → PK and PK → S1). The solid line through the experimental data represents a fit to a model which attributes the entire dependence of ΔG_{37} on solution pH to a single protonatable group on the RNA (see Materials and Methods). The parameters derived from the fits are compiled in Table 1.

pseudoknot, only slightly lower than that of the unmodified BWYV pseudoknot [p$K_a = 7.3$ (±0.4)]. The fully protonated m^5-C_8-BWYV pseudoknot is also ≈1.1 kcal mol^{-1} less stable than the unmodified BWYV pseudoknot at pH 7.0, most of which is associated with the relative stabilities of the protonated forms (Table 1).

Thermodynamic Evidence for Conservation of Structure in the PLRV Pseudoknot. On the basis of sequence (Figure 1) and functional similarities (*27*) to the BWYV pseudoknot, the PLRV pseudoknot was expected to be stabilized by the presence of loop L2−stem S1 minor groove and loop L1−stem S2 major groove triplex interactions. Consistent with these expectations, the calorimetrically monitored unfolding of the PLRV pseudoknot as a function of pH (Figure 4) reveals a total $\Delta H \approx 120$ kcal mol^{-1}, essentially identical to the unfolding enthalpy of the BWYV pseudoknot, and in large excess of the 63−70 kcal mol^{-1} of enthalpy anticipated for unfolding of the helical stems of the PLRV pseudoknot based on INN-HB rules (*27*). Deconvolution of the calorimetrically monitored unfolding of the PLRV pseudoknot upon application of the same sequential interacting model reveals that the loop−stem interactions of the PLRV pseudoknot contribute $\Delta H = 32$ kcal mol^{-1} to the stability of the folded pseudoknot, while protonation of the C_8^+•(G_{12}-C_{27}) triple base pair contributes ≥2.5 kcal mol^{-1} in stability at 37 °C by DSC (Figure 4, legend), coupled with an elevated p$K_a = 6.9$ (±0.3) (Table 1).[3] These findings are fully compatible with detailed NMR analysis of the PLRV pseudoknot, which reveals a 2D NOE spectrum that is essentially superimposable on the BWYV pseudoknot (P. Nixon and D. Giedroc, unpublished observations).

Thermodynamic Evidence for Conservation of Structure in the PEMV-1 Pseudoknot. The PEMV-1 pseudoknot incorporates a transversion in the sequence of loop L1 where the loop L1 cytidine (C_8 in the BWYV pseudoknot) is moved to the 3′ loop position with a uridine in place of the conserved cytidine at the 5′ side of loop L1. In addition, the putative accepting pair for the Hoogsteen C^+•(G-C) triple (C_{13}-G_{28}) is inverted relative to the other members of the luteovirus family pseudoknots (G_{12}-C_{26} in the BWYV pseudoknot) (Figure 1). Given the previously described functional (*16*) and thermodynamic studies (*13*), these sequence changes were expected to abolish the pH dependence of the unfolding of the PEMV-1 pseudoknot.

The calorimetrically monitored unfolding of the PEMV-1 pseudoknot (Figure 5) reveals that, contrary to these expectations, the RNA is characterized by an unfolding enthalpy in excess of the INN-HB predictions ($\Delta H \approx 109$ kcal mol^{-1}) and a strongly pH-dependent stability, with $\Delta(\Delta G)_{37}$ for protonation of 2.1 (±0.2) kcal mol^{-1} (Table 1). It is interesting to note that, at pH values below 7.0, the unfolding of the tertiary structure and stem S2 of the PEMV-1 pseudoknot become coincident or so tightly coupled that they are best modeled by a single, cooperative transition. The ΔH of 52 kcal mol^{-1} is near that determined for the sum of tertiary structure and S2 unfolding resolved at pH 7.0 and 8.0 ($\Delta H_{F\rightarrow PK+PK\rightarrow S1} = 55.8 \pm 1.0$ kcal mol^{-1}). Optically monitored melts are also characterized by significant pH dependence (melts not shown) (Table 1). A simultaneous analysis of pH dependence of the optical and calorimetric data like that applied to analyze the BWYV and PLRV RNA melts reveals a macroscopic pK_a of 7.1 (±0.2) (Figure 6).

[3] It proved impossible to deconvolute the first and second unfolding transitions from optical melts of the PLRV pseudoknot, precluding a thorough thermodynamic analysis of these data.

Table 1: Thermodynamic Parameters for the pH-Dependent Unfolding of the Luteoviral Pseudoknots[a]

RNA	$\Delta G_{37}^{protonated}$ (kcal mol^{-1})	$\Delta G_{37}^{unprotonated}$ (kcal mol^{-1})	$\Delta\Delta G_{37}^{protonation}$ (kcal mol^{-1})	pK_a	$\Delta G_{37}^{7.0}$ (kcal mol^{-1})[b]
BWYV	6.8 (±0.3)	3.7 (±0.3)	3.1 (±0.4)	7.3 (±0.3)	5.8 (±0.3)
dC_{14} BWYV	6.4 (±0.3)	3.8 (±0.2)	2.6 (±0.4)	5.7 (±0.3)	4.0 (±0.2)
m^5-C_8-BWYV	5.8 (±0.3)	4.0 (±0.2)	1.8 (±0.4)	6.7 (±0.4)	4.7 (±0.5)
PLRV[c]	3.2 (±0.2)	2.1 (±0.1)	1.1 (±0.1)	6.9 (±0.3)	2.5 (±0.5)
PEMV-1	4.9 (±0.2)	2.8 (±0.1)	2.1 (±0.2)	7.1 (±0.2)	3.7 (±0.4)
C_{11}-G_{30} PEMV-1	3.4 (±0.2)	1.1 (±0.3)	2.3 (±0.3)	8.0 (±0.2)	3.5 (±0.1)

[a] Summed from ΔG_{37} derived for unfolding transitions 1 and 2. ΔG_{37} for transition 3 was found to be independent of pH and was 7.7 (±0.5), 7.2 (±0.2), 7.8 (±0.3), 7.8 (±0.3), 5.6 (±0.1), and 5.7 (±0.1) kcal mol^{-1} for the BWYV, dC_{14} BWYV, m^5-C_8-BWYV, PLRV, PEMV-1, and C_{11}-G_{30} PEMV RNAs. [b] Experimentally determined, not fitted. [c] All ΔG_{37} values for the PLRV pseudoknot refer to those derived from unfolding transition 1 (ΔG_1), not the sum $\Delta G_1 + \Delta G_2$;[3] this particularly underestimates $\Delta\Delta G_{37}^{protonation}$ since these unfolding transitions are obligatorily coupled (see text for details).

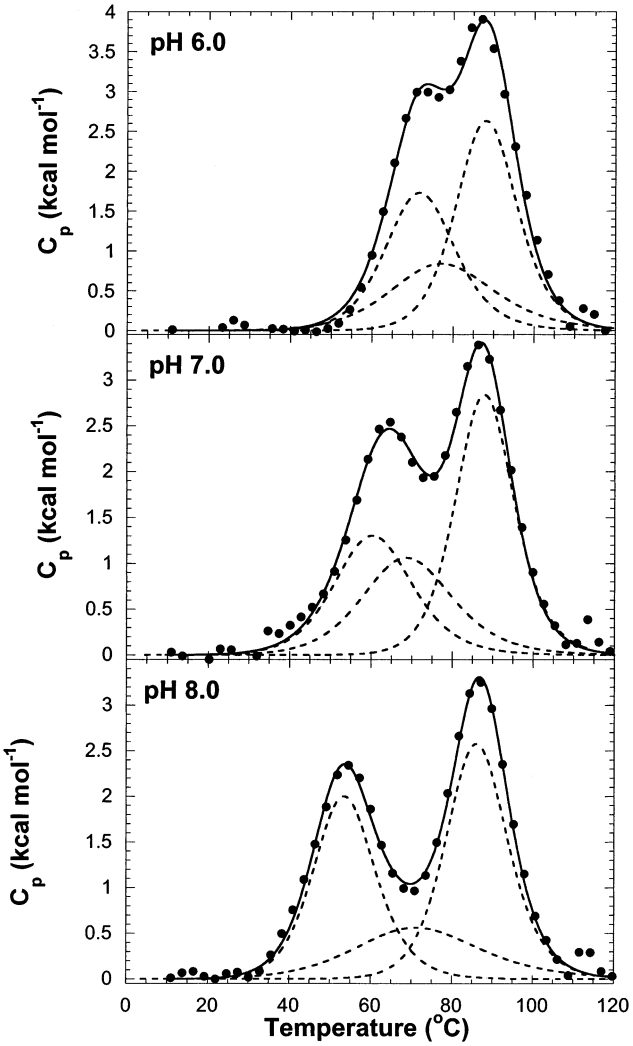

FIGURE 4: Calorimetrically monitored unfolding of the PLRV P1−P2 pseudoknot at pH 6.0, 7.0, and 8.0 in 0.5 M KCl and 10 mM buffer salt (see Materials and Methods). Sample concentrations were 46.0, 45.1, and 47.9 μM, respectively. For clarity, only 5% of the collected data points are shown in each panel with both the composite fit (solid line) and the individual transitions (dotted lines) superimposed on the data. Calculated thermodynamic parameters (in kcal mol^{-1}) for the unfolding of the PLRV pseudoknot obtained from fitting to a model of three sequential interacting transitions are as follows: pH 6.0, $\Delta H_{F\rightarrow PK} = 33.0$, $\Delta H_{total} = 123$, $\Delta G_{37(total)} = 14.7$, $\Delta G_{37(F-PK)} = 3.3$; pH 7.0, $\Delta H_{F\rightarrow PK} = 33.2$, $\Delta H_{total} = 122$, $\Delta G_{37(total)} = 13.1$, $\Delta G_{37(F-PK)} = 2.4$; pH 8.0, $\Delta H_{F\rightarrow PK} = 30.7$, $\Delta H_{total} = 121$, $\Delta G_{37(total)} = 11.4$, $\Delta G_{37(F-PK)} = 1.3$.

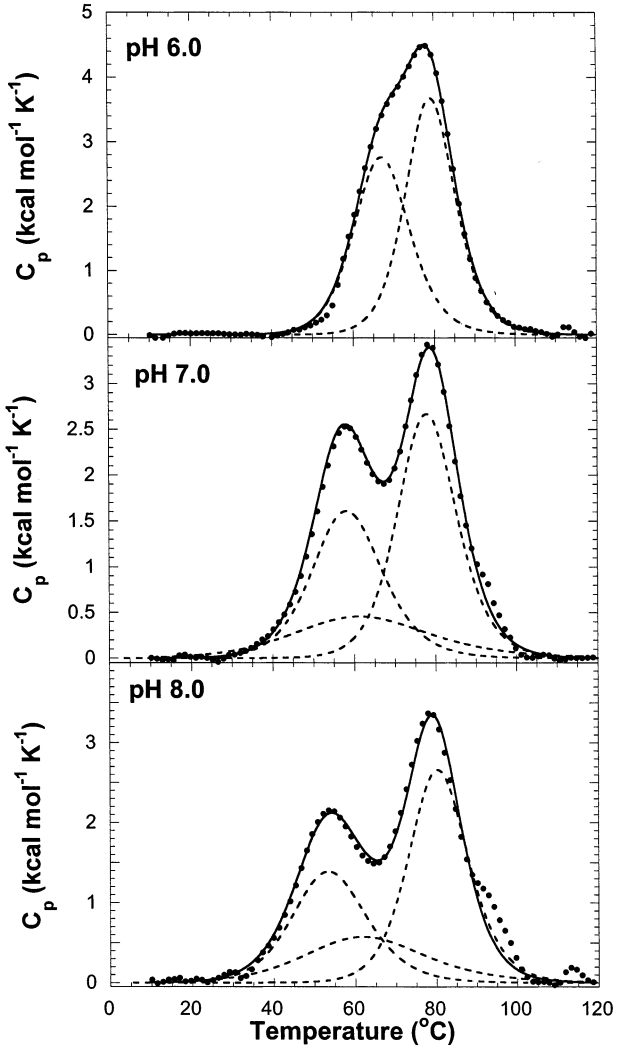

FIGURE 5: Calorimetrically monitored unfolding of the PEMV-1 pseudoknot at pH 6.0, 7.0, and 8.0 in 500 mM KCl and 10 mM buffer salt (see Materials and Methods). Sample concentrations were 85.0, 88.8, and 83.7 μM, respectively. For clarity, only 5% of the collected data points are shown in each panel with both the composite fit (solid line) and the individual transitions (dotted lines) superimposed on the data. Calculated thermodynamic parameters (in kcal mol^{-1}) for the unfolding of the PEMV-1 pseudoknot obtained from fitting to a model of three sequential interacting transitions are as follows: pH 6.0, $\Delta H_{F\rightarrow S1} = 52.0$, $\Delta H_{total} = 112$, $\Delta G_{37(total)} = 11.9$, $\Delta G_{37(F-S1)} = 4.7$; pH 7.0, $\Delta H_{F\rightarrow PK} = 37.0$, $\Delta H_{total} = 109$, $\Delta G_{37(total)} = 10.2$, $\Delta G_{37(F-PK)} = 2.4$; pH 8.0, $\Delta H_{F\rightarrow PK} = 30.0$, $\Delta H_{total} = 107$, $\Delta G_{37(total)} = 9.3$, $\Delta G_{37(F-PK)} = 1.3$.

This likely corresponds to apparent pK_a of the N_3H^+ imino proton of C_{10} in loop L1.

NMR and Thermodynamic Evidence for a C_{10}^+·(C_{13}-G_{28}) Base Triple in the PEMV-1 Pseudoknot. Since the tertiary

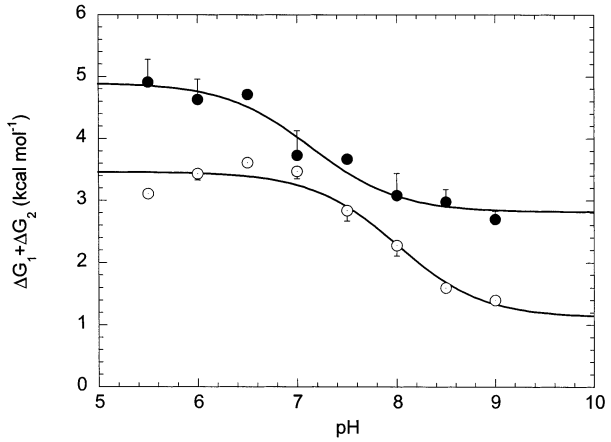

FIGURE 6: pH dependence on the unfolding of the wild-type (●) and mutant C_{11}-G_{30} (○) PEMV-1 pseudoknots. The average (±SD) $\Delta G_1 + \Delta G_2$ values derived from four independent optical melting experiments acquired at each pH value, except that $\Delta G_1 + \Delta G_2$ determined at pH 6.0, 7.0 and 8.0 for the wild-type PEMV-1 pseudoknot also incorporates results from DSC (cf. Figure 5). The solid line through each set of data corresponds to a fit to an equation which describes the entire dependence as attributable to a single protonatable group (see Materials and Methods). The parameters obtained from this analysis are compiled in Table 1.

structure of the PEMV-1 pseudoknot is strongly dependent on solution pH, three possibilities exist for the participation of C_{10} in a protonated L1−S2 triple base pair, analogous to that of the BWYV and PLRV pseudoknots (Figure 7). One is a C_{10}^+•(G_{11}-C_{30}) triple which would be isostructural with the BWYV C_8^+•(G_{12}-C_{26}) base triple (Figure 7A), simply moved away from the helical junction to the base of S2 (Figure 7B). Two other base triple structures are possible (Figure 7C,D). The C_{10}^+•(A_{12}-U_{29}) triple (Figure 7C) seems unlikely due to formation of only a single protonated C_{10} N_3H^+···O4 U_{29} hydrogen bond and no hydrogen bonds to the C_{10}^+ amino protons, a structure difficult to rationalize with the strongly downfield-shifted, nondegenerate chemical shifts of these two protons (cf. Figure 8). The other possibility (Figure 7D) is that the entire C_{10} nucleotide is "flipped over", analogous to that previously observed for the biotin-binding pseudoknot (*31*), which would enforce a local change in the polarity of the polynucleotide backbone; in this arrangement, C_{10} is in a position to form the same set of hydrogen bonds of the C_8^+•(G_{12}-C_{26}) base pair in the BWYV pseudoknot with the Hoogsteen face of the *inverted* C_{13}-G_{28} base pair at the helical junction. NMR spectroscopy and thermodynamic analysis of the wild-type PEMV-1 pseudoknot and two variant RNAs, U_{10} and C_{11}-G_{30}, were carried out to distinguish among these possibilities.

Figure 8 (top spectrum) reveals that the wild-type PEMV-1 pseudoknot is characterized by the correct number of imino proton resonances consistent with a pseudoknotted structure;[2] furthermore, this RNA exhibits a pair of downfield-shifted amino protons indicative of the presence of a protonated cytidine, assigned to C_{10}.[2] Although there are some significant chemical shift changes, the exchangeable proton region of the base pair inverted C_{11}-G_{30} PEMV-1 RNA yields substantially the same spectrum, including the presence of the downfield-shifted amino protons associated with protonated C_{10} (Figure 8, middle spectrum). Thus, it is unlikely that the closing G_{11}-C_{30} base pair is the triple base pair

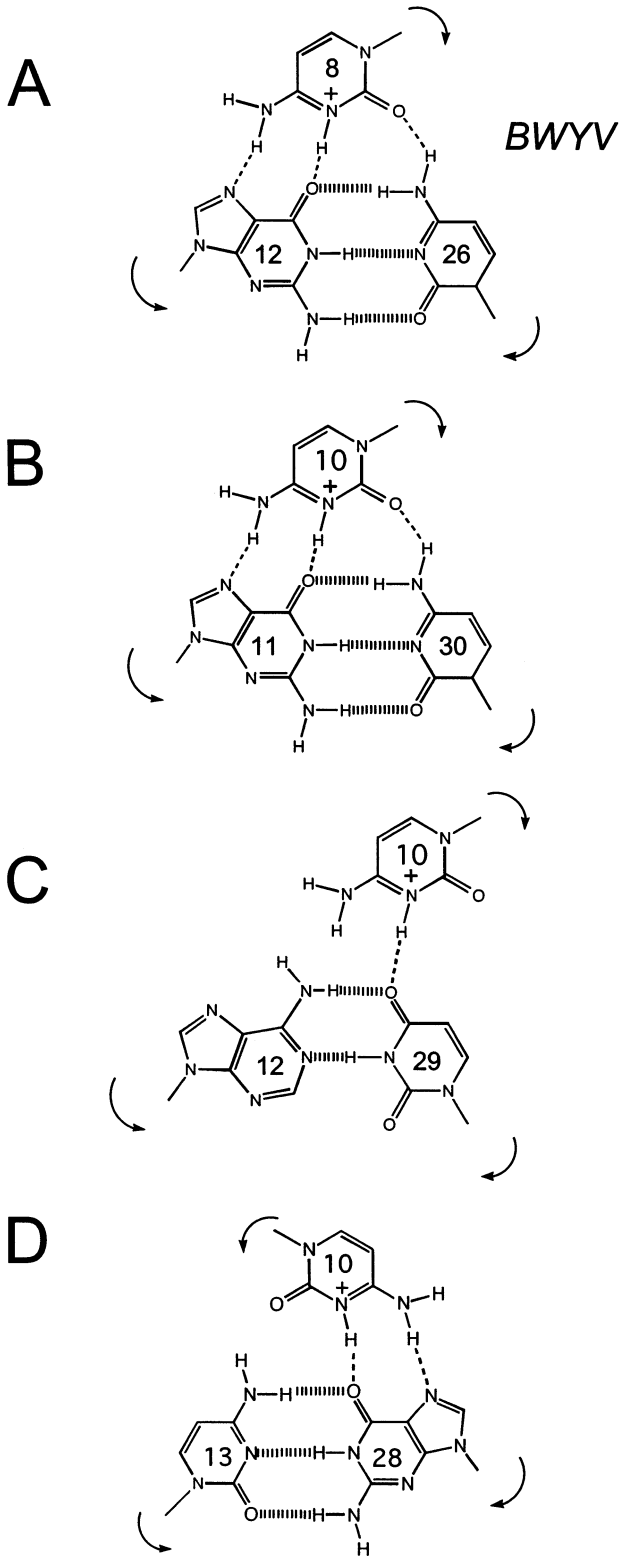

FIGURE 7: Schematic representation of the possible protonated triple base pairs that could be formed between a protonated C_{10} (L1) and the stem S2 base pairs in the PEMV-1 pseudoknot (panels B−D) compared to that of the wild-type BWYV base triple (panel A). See text for details.

acceptor, ruling out the model in Figure 7B. Consistent with this, the unfolding of the C_{11}-G_{30} PEMV-1 pseudoknot, while lowered as a result of the terminal base pair inversion, remains dependent on pH, with a macroscopic pK_a of 8.0 (±0.2) (Figure 6, Table 1). Interestingly, the stabilities of

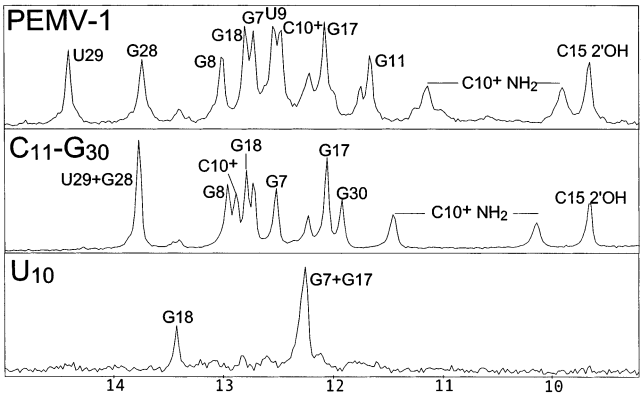

FIGURE 8: 1D NMR spectra (256 transients) of the exchangeable proton region of the wild-type (1.1 mM), C_{11}-G_{30} (1.5 mM), and U_{10} (0.5 mM) PEMV-1 RNAs at 1 °C, pH 6.0, and 0.10 M KCl. Complete proton resonance assignments for the PEMV-1 RNA pseudoknot have been deposited in the BMRB (deposition 5278).[2] The minor resonances at ≈12.2 and ≈13.4 ppm in the PEMV-1 spectrum derive from a small amount of contaminating 3′ truncated RNA which only folds into an S1 hairpin (cf. the U_{10} spectrum). The downfield shoulder on the peak labeled G11 (≈11.8 ppm) apparently derives from a distinct environment around the base of stem S2 in a minor conformation (data not shown), also observed in the analogous region of the phage T2 pseudoknot (*38*).

the wild-type and C_{11}-G_{30} PEMV-1 pseudoknots are indistinguishable at pH 7.0 (Table 1).

In contrast, the U_{10} PEMV-1 RNA does not adopt a folded RNA pseudoknot since only three imino protons are observed under these conditions, the expected number if the five base pair stem S1 is folded with the imino protons of the two terminal base pairs exchanging rapidly with solvent (Figure 8, bottom spectrum). The surprising conclusion is that the PEMV-1 pseudoknot conserves the stabilizing features of the BWYV/PLRV C^+·(G-C) triple base pair (Figure 7D) in a distinct structural context. Formation of this base triple appears to play a key role in nucleating other loop−stem interactions, e.g., a minor groove triplex, since substitution of C_{10} lowers the stability of the pseudoknot to a extent below that of the S1 hairpin (Figure 8, bottom spectrum).

Characterization of Loop L2 Substitution Mutants of the BWYV Pseudoknot. The other prominent structural feature of *Luteoviridae* P1−P2 pseudoknots is a minor groove triplex motif, in which loop L2 adenosines, particularly those at the 3′ end of loop L2, make functionally important (*16*) hydrogen-bonding interactions into the minor groove side of the G-C base pairs at the base of stem S1, near the helical junction (*9*). Structural and thermodynamic characterizations of $A_{23} \rightarrow G_{23}$, $A_{24} \rightarrow G_{24}$, and $A_{25} \rightarrow G_{25}$ and two 2′-deoxy BWYV substitution mutants, 2′-dC_{14} and 2′-dC_{15}, were undertaken to quantify the extent to which individual hydrogen-bonding interactions contribute to the stability of the BWYV pseudoknot.

1D NMR spectra of the exchangeable proton region for each of these RNAs are shown in Figure 9, compared to the spectrum of the wild-type BWYV pseudoknot (pH 6.0, 0.10 M K^+, 10 °C). Although only limited resonance assignments are available for the BWYV RNA, the presence or absence of the C_8^+ amino protons (see also Figure 2), coupled with the presence of the slowly exchanging 2′-OH of C_{14}, provides a qualitative indication of the extent to which the folded pseudoknotted conformation is the primary conformer under these conditions. These data reveal that substitution of A_{25}

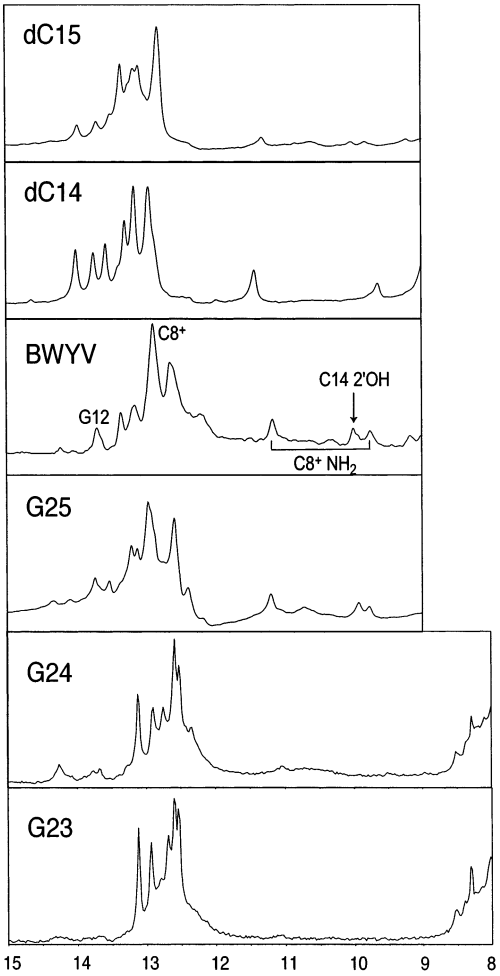

FIGURE 9: 1D NMR spectra (2048 transients) of the exchangeable proton region of the wild-type BWYV (0.6 mM), dC_{14} (0.7 mM), dC_{15} (1.1 mM), $A_{25}G$ (0.9 mM), $A_{24}G$ (1.1 mM), and $A_{23}G$ (1.2 mM) RNAs at 10 °C, pH 6.0, and 0.1 M KCl.

with G_{25} and replacement of the 2′-OH of C_{14} with a proton, i.e., the stabilizing elements closest to the helical junction, are tolerated by the pseudoknotted conformation. Consistent with this, thermal melting profiles of the 2′-dC_{14} RNA are well described by three unfolding transitions (Figure 10A); however, the RNA is destabilized by a $\Delta(\Delta G_{37}) \approx 1.8$ kcal mol^{-1} (pH 7.0, 0.5 M K^+) (Table 1) and is characterized by a downward-shifted pK_a of 5.7 (±0.4) relative to the wild-type RNA (Figure 10B). Thermal melts of the G_{25} RNA also show the presence of three unfolding transitions (data not shown). In contrast, the G_{24} and G_{23} BWYV RNAs give nearly identical NMR spectra and appear to be largely unfolded, with the G_{24} and the 2′-dC_{15} RNA best described as a mixture of folded and S1 hairpin conformers. Thus, disruption of minor groove interactions one S1 base pair or one L2 nucleotide removed from the helical junction is comparatively more destabilizing than are identical substitutions nearer the helical junction (see Discussion).

DISCUSSION

In the work described here, we provide thermodynamic and structural evidence that all members of the *Luteoviridae* P1−P2 mRNA frameshifting pseudoknots contain a common collection of loop−stem tertiary structural interactions that make integral contributions to the stability of the pseudoknot-

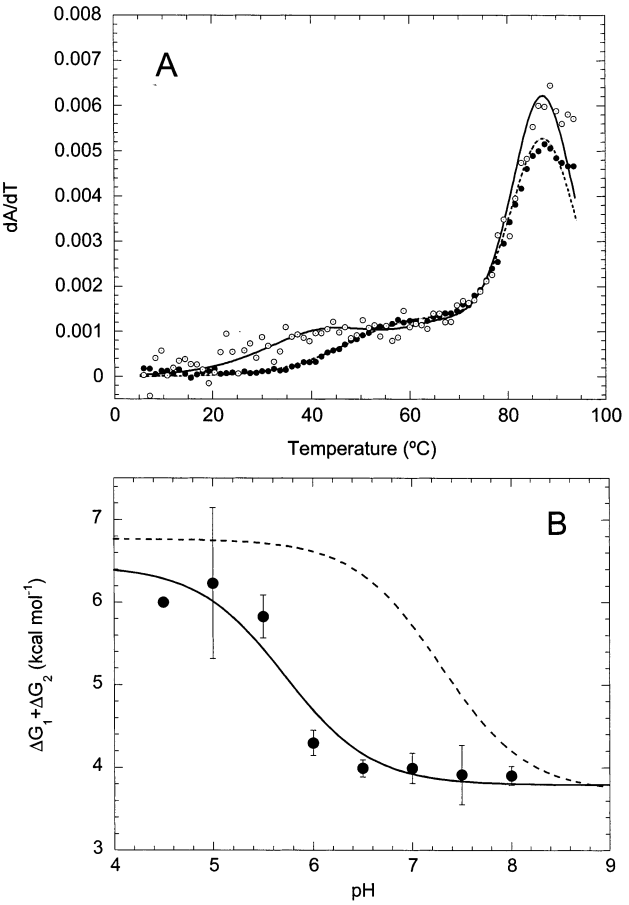

FIGURE 10: (A) Representative thermal melting profiles (dA_{260}/dT) obtained for dC_{14} BWYV RNA at pH 6.0 (●) and pH 8.0 (○) in 0.5 M KCl and 10 mM buffer salt (see Materials and Methods). The smooth curves superimposed on the data represent a simultaneous fit (both dA_{260}/dT and dA_{280}/dT were used; dA_{280}/dT is not shown for clarity) to a model of three sequential, interacting unfolding transitions (transitions 1−3) assigned to the unfolding of the pseudoknot tertiary structure, stem S2, and stem S1, respectively (*13*). (B) pH dependence on the unfolding of the dC_{14} BWYV pseudoknot. The average (±SD) $\Delta G_1 + \Delta G_2$ values (37 °C) derived from four independent optical melting experiments acquired at each pH value are shown. The solid line through the data corresponds to a fit to an equation which describes the entire dependence as attributable to a single protonatable group. The apparent pK_a determined from this analysis is 5.7 (±0.3) (Table 1). The pH dependence of the unfolding of the wild-type BWYV pseudoknot is shown (dashed line; cf. Figure 2) for comparison.

ted conformation relative to the partially unfolded S1 hairpin. This conclusion is fully compatible with functional studies of mutant BWYV (*16*), PLRV (*17*), and PEMV-1[2] pseudoknots; any disruption of these stabilizing tertiary structural interactions was found to be generally deleterious to function.

The C^+·(G-C) Base Triple. The C^+·(G-C) major groove base triple motif is a common feature of all luteoviral pseudoknots, despite nucleotide sequence changes in the PEMV-1 RNA which would be expected to abolish this interaction. In all cases, the global stability of the pseudoknot is markedly pH-dependent with a pK_a of unfolding markedly elevated relative to that of free cytidine, such that significant protonation of the loop L2 cytidine N3 occurs at neutral pH. The thermodynamic driving force for the elevated pK_a is not known with certainty although the structures of the BWYV (*9*) and PEMV-1[2] pseudoknots reveal that while one face of the protonated cytidine is largely exposed to solvent, the other is nearby a patch of significant negative electrostatic potential deep in the major groove of S2. The same is true of the C^+·(G-C) base triple in the genomic HDV ribozyme (*11*). Protonation may therefore be important for enhancing electrostatic complementarity in the major groove of S2. Regardless of the molecular origin, protonation of the loop L1 cytidine makes a significant contribution to the global stability with a $\Delta(\Delta G_{37})_{folding}$ of 3.1 (±0.3) and ≥2.5 kcal mol^{-1} for the BWYV and PLRV[3] pseudoknots, respectively, and slightly less, 2.1 (±0.3) kcal mol^{-1}, to the stability of the PEMV-1 RNA.

As anticipated, replacement of C_8 with m^5-C_8 in the BWYV pseudoknot is fully compatible with formation of the pseudoknot (Figure 2), with $\Delta(\Delta G_{37})_{folding}$ of ≈1.1 (±0.5) kcal mol^{-1} at pH 7.0 (Table 1) relative to that of the unmethylated RNA. Although the effect is small (Figure 3), at least some of the difference in stability between the BWYV and m^5-C_8-BWYV pseudoknots at pH 7.0 is due to a small downward shift in the macroscopic pK_a for pseudoknot unfolding (Table 1), in a direction opposite to expectations based on the relative pK_a's of free cytidine (pK_a ≈ 4.2) and free 5-methylcytidine (pK_a ≈ 4.4) (*30*). It is important to recognize that the pK_a for (un)folding is an apparent pK_a that measures the microscopic pK_a superimposed on changes in base stacking and hydrophobicity and electrostatics (*32*), as well as other coupled protonation/deprotonation equilibria, which might influence the global unfolding equilibrium.

Thermodynamic and Structural Analysis of Loop L2 Mutants in the BWYV Pseudoknot: Cooperativity of Weak Interactions. From the thermodynamic data alone, both the PLRV and PEMV-1 pseudoknots were expected to contain a comprehensive collection of loop−stem minor groove interactions; the solution structure of the PEMV-1 pseudoknot is consistent with this expectation.[2] In addition, the NMR spectra of both the BWYV (Figure 9) and the PEMV-1 (Figure 8) pseudoknots reveal that the 2′-hydroxyl protons of C_{14} in BWYV and the analogous nucleotide (C_{15}) in PEMV-1 are significantly downfield-shifted and exchange very slowly with solvent,[2] evidence that they are involved in donating hydrogen bonds to L2 adenosines in solution. In an effort to define the extent to which each of these interactions contributes to the stability of the pseudoknotted conformation, $A_{23}G$, $A_{24}G$, and $A_{25}G$ BWYV RNAs, as well as two 2′-deoxy RNAs, dC_{14} and dC_{15}, were characterized.

We find that the dC_{14} BWYV RNA is indeed folded and destabilized to an extent compatible with previous studies of the *T. thermophilus* P4−P6 group I intron domain (*10*) [$\Delta(\Delta G_{37})_{folding}$ ≈ 1.2 kcal mol^{-1}], with $\Delta(\Delta G_{37})_{folding}$ ≈ 1.8 (±0.5) kcal mol^{-1} at pH 7.0, coupled with a significant reduction in the apparent pK_a of C_8 (Figure 10, Table 1). In strong contrast, the dC_{15} RNA is substantially unfolded under these conditions, with only a minor population of molecules adopting a pseudoknotted conformation as defined by the intensity of the protonated C_8^+ amino protons (Figure 9). The same is true of the $A_{25}G$ RNA. In contrast, the structure of the $A_{24}G$ and $A_{23}G$ RNAs are significantly perturbed with little evidence of a stable folded pseudoknot. Knowledge of the relative stabilities of the pseudoknot and partially folded S1 hairpin reveals a $\Delta(\Delta G_{37})_{folding}$ of ≈7 kcal mol^{-1} at low pH vs ≈4 kcal mol^{-1} at elevated pH (Table 1). Thus, a lower limit for $\Delta(\Delta G_{37})_{folding}$ which characterizes these A → G base substitutions as well as the replacement of a single 2′-OH

with a 2′-H group in C_{15} is ≥4 kcal mol^{-1} under these solution conditions, compatible with previous findings for globally stabilizing A → G substitutions the P4−P6 domain of the group I intron (*10*).

Implications for RNA Folding. In the absence of stabilizing interactions associated specifically with A_{23}, A_{24}, and the G_6-C_{15} S1 base pair, a large-scale perturbation of complementarity of loop−stem interactions results, which, when not allowed to form, subsequently abolishes the formation of other stabilizing interactions nearer the helical junction and perhaps through stem S2. This has the effect of coupling the formation of the minor groove triplex with the formation of the relatively weak three base pair stem S2, which itself is further stabilized by protonation of an L1 nucleotide. Molecular dynamics simulations carried out at elevated temperature (400 K) provide additional evidence for strong *temporal* coupling of disruption of the C_8^+•G_{12} Hoogsteen pair with that of the minor groove triplex (*33*); along the folding coordinate, this would obligatorily couple formation of the minor groove triplex with the C_8^+•(G_{12}-C_{26}) base triple. Thus, A_{23} and A_{24} may therefore play important roles in nucleating a strong cooperativity of subsequent interactions along the kinetic folding reaction coordinate as well.

Functional Implications. These and previous studies reveal a strong correlation between the formation of the major C^+• (G-C) triple base pair and a minor groove triplex and the ability of *Luteoviridae* P1−P2 pseudoknots to stimulate programmed −1 ribosomal frameshifting in vitro (*16*, *17*).[2] Indeed, it is not difficult to understand how mutations that shift the folding equilibrium toward the S1 hairpin would abolish stimulation of frameshifting activity. However, what is not so clear is how small changes in the stability of a loop−stem tertiary structural motif nearer the helical junction, for example, could account for the large reductions in frameshifting efficiency. The role of the protonated C^+•(G-C) triple in stimulating ribosomal frameshifting is a case in point. If it were simply the protonation state or stability derived from this interaction which were responsible for stimulation of frameshifting efficiencies, in vitro frameshifting assays would not likely have detected this, since these experiments are typically carried out at pH 7.8,[4] a pH at which the luteoviral pseudoknots are predicted to be near minimal stability (Table 1). Despite this, mutations which disrupt the pH dependence of the C^+•(G-C) base triple but do not abolish pseudoknot formation, e.g., U_8 BWYV pseudoknot, result in an apparently complete loss in the ability to stimulate frameshifting (*16*) with a relatively small loss of thermodynamic stability at elevated pH (*13*). A similar argument could also be made for the A_{25}G substitution, which is also functionally completely inactive (*16*).

Other studies suggest that there is unlikely to be simple relationship between the stability of the pseudoknot relative to the partially folded hairpin conformation and efficiency of stimulating −1 frameshifting, beyond that which is required to ensure that the pseudoknotted structure dominates the population ensemble (*4*).[5] Similar conclusions have been reached from studies of the HIV-1 *gag-pol* and HTLV-II *gag-pro* stem−loop structures, which showed little to no correlation between functional activity and predicted RNA stem−loop stability (*34*). On the other hand, recent evidence from the MMTV *gag-pro*, IBV-MMTV chimeric, and SRV-1 *gag-pro* pseudoknot systems suggests that weakly stabilizing structural determinants positioned at the helical junction may play a far more significant role in stimulation of frameshifting activity as the pseudoknot abuts the elongating ribosome than will global stability (*35*−*37*).[5] It will be necessary to elucidate the kinetics of pseudoknot unfolding and refolding, as well as the structural nature of the transient interactions of the pseudoknot with the ribosome, before a detailed understanding of the mechanism of translational regulation of gene expression by programmed −1 ribosomal frameshifting can be obtained.

[4] Promega Technical Support, personal communication.

[5] E. Sulistijo, B. Cannon, C. Theimer, and D. Giedroc, unpublished observations.

REFERENCES

1. Farabaugh, P. J. (1993) *Cell 74*, 591−596.
2. Matsufuji, S., Matsufuji, T., Wills, N. M., Gesteland, R. F., and Atkins, J. F. (1996) *EMBO J. 15*, 1360−1370.
3. Gesteland, R. F., and Atkins, J. F. (1996) *Annu. Rev. Biochem. 65*, 741−768.
4. Giedroc, D. P., Theimer, C. A., and Nixon, P. L. (2000) *J. Mol. Biol. 298*, 167−185.
5. Jacks, T., Madhani, H. D., Masiarz, F. R., and Varmus, H. E. (1988) *Cell 55*, 44−58.
6. Lopinski, J. D., Dinman, J. D., and Bruenn, J. A. (2000) *Mol. Cell. Biol. 20*, 1095−1103.
7. Somogyi, P., Jenner, A. J., Brierley, I., and Inglis, S. C. (1993) *Mol. Cell. Biol. 13*, 6931−6940.
8. Gultyaev, A. P., van Batenburg, F. H., and Pleij, C. W. (1999) *RNA 5*, 609−617.
9. Su, L., Chen, L., Egli, M., Berger, J. M., and Rich, A. (1999) *Nat. Struct. Biol. 6*, 285−292.
10. Doherty, E. A., Batey, R. T., Masquida, B., and Doudna, J. A. (2001) *Nat. Struct. Biol. 8*, 339−343.
11. Ferre-D'Amare, A. R., and Doudna, J. A. (2000) *J. Mol. Biol. 295*, 541−556.
12. Wadkins, T. S., Shih, I.-h., Perrotta, A. T., and Been, M. D. (2001) *J. Mol. Biol. 305*, 1045−1055.
13. Nixon, P. L., and Giedroc, D. P. (2000) *J. Mol. Biol. 296*, 659−671.
14. Miller, A. W., Dinesh-Kumar, S. P., and Paul, C. P. (1995) *Crit. Rev. Plant Sci. 13*, 179−211.
15. Wobus, C. E., Skaf, J. S., Schultz, M. H., and de Zoeten, G. (1998) *J. Gen. Virol. 79*, 2023−2025.
16. Kim, Y.-G., Su, L., Maas, S., O'Neill, A., and Rich, A. (1999) *Proc. Natl. Acad. Sci. U.S.A. 96*, 14234−14239.
17. Kim, Y.-G., Maas, S., Wang, S. C., and Rich, A. (2000) *RNA 6*, 1157−1165.
18. Paul, C. P., Barry, J. K., Dinesh-Kumar, S. P., Brault, V., and Miller, W. A. (2001) *J. Mol. Biol. 310*, 987−999.
19. Brault, V., and Miller, W. A. (1992) *Proc. Natl. Acad. Sci. U.S.A. 89*, 2262−2266.
20. Puglisi, J. D., Wyatt, J. R., and Tinoco, I., Jr. (1990) *J. Mol. Biol. 214*, 437−453.
21. Stump, W. T., and Hall, K. B. (1993) *Nucleic Acids Res. 21*, 5480−5484.
22. Jorgensen, E. D., Durbin, R. K., Risman, S. S., and McAllister, W. T. (1991) *J. Biol. Chem. 266*, 645−651.
23. Nixon, P. L., and Giedroc, D. P. (1998) *Biochemistry 37*, 16116−16129.
24. Conn, G. L., Gutell, R. R., and Draper, D. E. (1998) *Biochemistry 37*, 11980−11988.
25. Theimer, C. A., and Giedroc, D. P. (1999) *J. Mol. Biol. 289*, 1283−1299.
26. Delaglio, F., Grzesiek, S., Vuister, G. W., Zhu, G., Pfeifer, J., and Bax, A. (1995) *J. Biomol. NMR 6*, 277−293.
27. Xia, T., SantaLucia, J., Jr., Burkard, M. E., Kierzek, R., Schroeder, S. J., Jiao, X., Cox, C., and Turner, D. H. (1998) *Biochemistry 37*, 14719−14735.
28. Draper, D. E. (1996) *Trends Biochem. Sci. 21*, 145−149.
29. Wijmenga, S. S., and Van Buuren, B. N. M. (1998) *Prog. Nucl. Magn. Reson. Spectrosc. 32*, 287−387.

30. Hall, R. H. (1971) in *The Modified Nucleosides in Nucleic Acids*, Columbia University Press, New York.
31. Nix J., Sussman, D., and Wilson, C. (2000) *J. Mol. Biol. 296*, 1235−1244.
32. Leitner, D., Schröder, W., and Weisz, K. (2000) *Biochemistry 39*, 5886−5892.
33. Csaszar, K., Spackova, N., Stefl, R., Sponer, J., and Leontis, N. B. (2001) *J. Mol. Biol. 313*, 1073−1091.
34. Kim, Y-.G., Maas, S., and Rich, A. (2001) *Nucleic Acids Res. 29*, 1125−1131.
35. Theimer, C. A., and Giedroc, D. P. (2000) *RNA 6*, 409−421.
36. Michiels, P. J. A., Versleijen, A. A. M., Verlaan, P. A., Pleij, C. W. A., Hilbers, C. W., and Heus, H. A. (2001) *J. Mol. Biol. 305*, 1109−1123.
37. Liphardt, J., Napthine, S., Kontos, H., and Brierley, I. (1999) *J. Mol. Biol. 288*, 321−335.
38. Du, Z., Giedroc, D. P., and Hoffman, D. W. (1996) *Biochemistry 35*, 4187−4198.

BI025843C